Degenerate two-level system in the presence of a transverse magnetic field

L. Margalit,[1] M. Rosenbluh,[2] and A. D. Wilson-Gordon[1]
[1]*Department of Chemistry, Bar-Ilan University, Ramat Gan 52900, Israel*
[2]*The Jack and Pearl Resnick Institute for Advanced Technology, Department of Physics, Bar-Ilan University, Ramat-Gan 52900, Israel*
(Received 2 December 2012; published 12 March 2013)

The effect of a transverse magnetic field (TMF) on the absorption spectra of degenerate two-level systems in the D_2 line of ^{87}Rb is investigated both analytically and numerically. We compare the effect of the TMF on the absorption of a σ polarized pump in the Hanle configuration with that of a σ^- probe in the presence of a σ^+ pump in the pump-probe configuration, and we show that the absorption spectra in both configurations is split in the presence of a TMF and that the splitting is proportional to its magnitude. The population redistribution in the ground state due to the TMF is reinforced by collisional effects, leading to increased splitting of the coherent population trapping (CPT) dip in the absorption spectrum. We explain the appearance of the splitting by setting the quantization axis along the total magnetic field. Then, in the Hanle configuration, the direction of the quantization axis changes as the longitudinal magnetic field is scanned, so that the laser polarization also changes. This leads to the creation of new two-photon detuned Λ subsystems. The evolution of the populations and coherences of the ground-state Zeeman sublevels is illustrated using the angular momentum probability surface. In addition to being split, the CPT dip in the pump-probe configuration is also shifted by the longitudinal magnetic field, so that the effects of the longitudinal and transverse magnetic fields can be distinguished from each other.

DOI: 10.1103/PhysRevA.87.033808 PACS number(s): 42.50.Gy, 32.80.Xx, 32.70.Jz

I. INTRODUCTION

The effect of a transverse magnetic field (TMF), defined as a magnetic field perpendicular to the propagation direction of the excitation light, on the absorption and fluorescence spectra of degenerate two-level systems (DTLSs) in alkali metals has been investigated in the past, both experimentally and theoretically, using the Hanle configuration, in which the magnetic field is scanned through zero. Systems characterized by coherent population trapping (CPT) [1–5], electromagnetically induced transparency (EIT) [6], and electromagnetically induced absorption (EIA) [6–10] have been studied. These studies can be divided into those in which the longitudinal magnetic field is scanned in the presence of a constant TMF [1,2,4,6,8,10] and those where the TMF is scanned in the presence or absence of a constant longitudinal field [3,6,7,9]. The influence of a TMF on the spectrum when the longitudinal magnetic field, parallel to the light propagation direction, is scanned has been investigated in Rb for excitation with linear, circular, and elliptical laser polarizations [1] and in Cs with laser light having various elliptical polarizations [2]. It was shown that the TMF can enhance or reduce the CPT amplitude depending on the orientation of the TMF with respect to the laser polarization [1,2]. In the case of σ laser polarization, the TMF causes a reduction in the amplitude of the CPT resonance and an increase in its width in a nonlinear manner [1]. It has been shown [9] that when the TMF is scanned the Hanle resonance of a σ^- probe in the presence of a σ^+ polarized pump undergoes a change of sign as the pump intensity increases. A similar effect was reported for counterpropagating linearly polarized pump and probe beams when the longitudinal magnetic field is scanned [11]. In this case, the Hanle resonance changes sign as the angle between the linear polarizations changes from 0 to 90°.

Various studies have shown that collisional effects can have a strong influence on the spectra observed in the presence of a TMF. For example, Renzoni *et al.* [7] showed that the amplitude and width of the Hanle EIA spectrum when the TMF is scanned are strongly dependent on the ground-state relaxation processes, and Yu *et al.* [4] assigned the changes in the Hanle absorption spectrum for a circularly polarized field in the presence of TMF to population redistribution, due both to the TMF and the increase in the atom-laser interaction time caused by the buffer gas in the cell.

There are two main theoretical approaches to dealing with the presence of a TMF in addition to a longitudinal magnetic field. In the first, the quantization axis is chosen to be along the total magnetic field [5,8,12], so that adding a TMF changes the orientation of the axes and thus the effective light polarization. The Zeeman shifts of the Zeeman sublevels in the Bloch equations [13] are then proportional to the total magnetic field.

The second approach is to set the axis of light propagation or B_z as the quantization axis and add extra terms to the Bloch equations [13] that relate to coupling between $\Delta m = \pm 1$ Zeeman sublevels due to the TMF [1,2,7,9,14]. In this approach, the Zeeman shift in the Bloch equations is proportional only to B_z. If the Hamiltonian matrix is diagonalized, new energy levels are obtained whose Zeeman shifts are proportional to the total applied magnetic field, as expected. Thus, the results obtained from the two approaches should be identical.

To our knowledge, the effect of the TMF on the pump-probe absorption spectra has not been investigated theoretically for DTLSs. This may be due to the fact that it is simpler to solve the equations when only one laser is applied, as in the Hanle configuration. In this paper, we calculate the effect of a TMF on the absorption of a σ polarized pump in the Hanle configuration, and we show that it is similar to calculating the effect of a TMF on a pump-probe configuration with a frequency tuned σ^- probe in the presence of a fixed frequency σ^+ pump in a fixed longitudinal magnetic field. For the pump-probe configuration, it is simpler to set the axis of light propagation as the quantization axis, since, for any other arbitrary quantization axis, the initial polarizations of

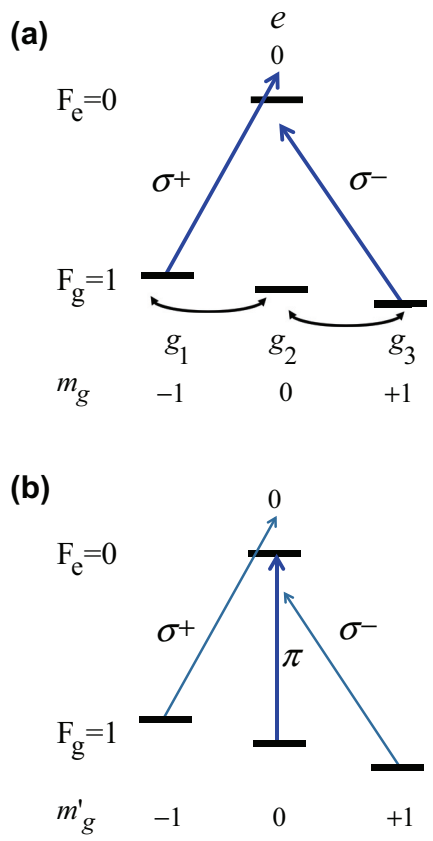

FIG. 1. (Color online) (a) The quantization axis set along the light propagation direction. (b) The quantization axis set along the total magnetic-field direction.

the pump and the probe are modified by the presence of the TMF and become combinations of σ^+, σ^-, and π, so that both fields interact with the same transitions, making the problem difficult to solve. Thus, in our calculations we set the axis of light propagation to be the quantization axis.

In the case of a pump-probe configuration, in which each field interacts with a different hyperfine transition, as in the three-level Λ system, the CPT spectrum can be easily calculated using an arbitrary quantization axis. In this case, the combination of σ^+, σ^-, and π polarizations in the presence of the TMF leads to the creation of multiple frequency displaced Λ systems and therefore to new resonances in the CPT spectra [12,15]. In [12,15], the quantization axis was chosen to be along the total magnetic field, and we have confirmed their results using the calculational model reported here, in which the quantization axis is set to be along the light propagation direction.

Here, we show both numerically and analytically that the absorption spectra in both the Hanle and pump-probe configurations for the $F_g = 1 \rightarrow F_e = 0$ transition (see Fig. 1) are split in the presence of a TMF and that the splitting is proportional to the magnitude of the TMF. We note that the splitting is more marked in the presence of collisions that reinforce the effect of population redistribution due to the mixing of the Zeeman sublevels by the TMF. As in the case of the degenerate three-level Λ system [12,15], the splitting can be explained as being due to the creation of new Λ subsystems formed by the Zeeman sublevels.

In addition to being split, the CPT line in the pump-probe configuration is shifted by the longitudinal magnetic field. Thus, we find that the effects of longitudinal and transverse magnetic fields can be distinguished from each other.

II. THE OPTICAL BLOCH EQUATIONS

Choosing the propagation axis z as the quantization axis, we write the Bloch equations for a system consisting of a ground hyperfine state F_g composed of $2F_g + 1$ Zeeman sublevels g_i and an excited hyperfine state F_e composed of $2F_e + 1$ Zeeman sublevels e_j, interacting with one or more electromagnetic fields in the presence of a constant longitudinal magnetic field. We use the equations for the time evolution of the Zeeman sublevels as formulated by Renzoni *et al.* [16], with the addition of decay from the ground and excited states to a reservoir [17], and collisions between atoms in the Zeeman sublevels of the ground states [18].

The optical Bloch equations have the following form:

$$\dot{\rho}_{e_i e_j} = -\left(i\omega_{e_i e_j} + \Gamma\right)\rho_{e_i e_j} + (i/\hbar)\sum_{g_k}\left(\rho_{e_i g_k} V_{g_k e_j} - V_{e_i g_k}\rho_{g_k e_j}\right) - \gamma\left(\rho_{e_i e_j} - \rho^{eq}_{e_i e_i}\right)\delta_{e_i e_j}, \tag{1}$$

$$\dot{\rho}_{e_i g_j} = -\left(i\omega_{e_i g_j} + \Gamma'_{e_i g_j}\right)\rho_{e_i g_j} + (i/\hbar)\left(\sum_{e_k}\rho_{e_i e_k} V_{e_k g_j} - \sum_{g_k} V_{e_i g_k}\rho_{g_k g_j}\right), \tag{2}$$

$$\dot{\rho}_{g_i g_i} = (i/\hbar)\sum_{e_k}\left(\rho_{g_i e_k} V_{e_k g_i} - V_{g_i e_k}\rho_{e_k g_i}\right) + \left(\dot{\rho}_{g_i g_i}\right)_{SE} - \gamma\left(\rho_{g_i g_i} - \rho^{eq}_{g_i g_i}\right) + \sum_{g_k, k\neq i}\Gamma_{g_k g_i}\rho_{g_k g_k} - \Gamma_{g_i}\rho_{g_i g_i}, \tag{3}$$

$$\dot{\rho}_{g_i g_j} = -\left(i\omega_{g_i g_j} + \Gamma'_{g_i g_j}\right)\rho_{g_i g_j} + (i/\hbar) \times \sum_{e_k}\left(\rho_{g_i e_k} V_{e_k g_j} - V_{g_i e_k}\rho_{e_k g_j}\right) + \left(\dot{\rho}_{g_i g_j}\right)_{\mathrm{SE}}, \tag{4}$$

where

$$\left(\dot{\rho}_{g_i g_j}\right)_{\mathrm{SE}} = (2F_e + 1)\Gamma_{F_e\rightarrow F_g}\sum_{q=-1,0,1}\ \sum_{m_e, m'_e=-F_e}^{F_e}(-1)^{-m_e - m'_e} \times \begin{pmatrix} F_g & 1 & F_e \\ -m_{g_i} & q & m_e \end{pmatrix}\rho_{m_e m'_e}\begin{pmatrix} F_e & 1 & F_g \\ -m'_e & q & m_{g_j} \end{pmatrix}, \tag{5}$$

with

$$\Gamma_{F_e\rightarrow F_g} = (2F_g + 1)(2J_e + 1)\begin{Bmatrix} F_e & 1 & F_g \\ J_g & I & J_e \end{Bmatrix}^2\Gamma \equiv b\Gamma. \tag{6}$$

In Eqs. (1)–(4), Γ is the *total* spontaneous emission rate from each $F_e m_e$ sublevel, whereas $\Gamma_{F_e\rightarrow F_g}$ is the decay rate from F_e to one of the F_g states. When $b = 1$ the system is closed, whereas when $b < 1$ the system is open. Γ_{g_i} is the total collisional decay rate from sublevel g_i, $\Gamma_{g_i g_j}$ is the rate of transfer from sublevel $g_i \rightarrow g_j$, and γ is the rate of decay due to time of flight through the laser beams. The dephasing rates

of the excited- to ground-state coherences are given by $\Gamma'_{e_i g_j} = \gamma + \frac{1}{2}(\Gamma + \Gamma_{g_j}) + \Gamma^*$, where Γ^* is the rate of phase-changing collisions. The dephasing rates of the ground-state coherences are given by $\Gamma'_{g_i g_j} = \gamma + \frac{1}{2}(\Gamma_{g_i} + \Gamma_{g_j}) + \Gamma^*_{g_i g_j}$, where $\Gamma^*_{g_i g_j}$ is the rate of phase-changing collisions. The Zeeman splitting $\Delta E_{m_F} = \mu_B g_F B_z m_F$ of the ground and excited levels due to an applied B_z magnetic field, where μ_B is the Bohr magneton and g_F is the gyromagnetic factor of the ground or excited state, is included in the frequency separation between the levels a_i and b_j, given by $\omega_{a_i b_j} = (E_{a_i} - E_{b_j})/\hbar$, with $a,b = (g,e)$. $\rho^{eq}_{a_i a_i}$ with $a = (g,e)$ is the equilibrium population of state a_i, in the absence of any electromagnetic fields.

In this paper, we solve the general Bloch equations in the steady state for two cases: (1) a pump of frequency ω_1 with σ polarization and a scanning longitudinal magnetic field B_z in the Hanle configuration and (2) a pump of frequency ω_1 with σ^+ polarization and a scanning probe of frequency ω_2 with σ^- polarization in the pump-probe configuration. In both cases, we consider the effect of an additional transverse magnetic field, for instance B_x. Thus, we include the following additional terms [7] in the Bloch equations:

$$\dot{\rho}_{e_i e_j}|_{B_x} = -i\frac{\mu_B B_x}{2\hbar} g_e \left\{ c^+_{e_i}\rho_{e_{i+1}e_j} + c^-_{e_i}\rho_{e_{i-1}e_j} - c^+_{e_j}\rho_{e_i e_{j+1}} - c^-_{e_j}\rho_{e_i e_{j-1}} \right\}, \tag{7}$$

$$\dot{\rho}_{e_i g_j}|_{B_x} = -i\frac{\mu_B B_x}{2\hbar} \left\{ g_e \left[c^+_{e_i}\rho_{e_{i+1}g_j} + c^-_{e_i}\rho_{e_{i-1}g_j} \right] - g_g \left[c^+_{g_j}\rho_{e_i g_{j+1}} + c^-_{g_j}\rho_{e_i g_{j-1}} \right] \right\}, \tag{8}$$

$$\dot{\rho}_{g_i g_j}|_{B_x} = -i\frac{\mu_B B_x}{2\hbar} g_g \left\{ c^+_{g_i}\rho_{g_{i+1}g_j} + c^-_{g_i}\rho_{g_{i-1}g_j} - c^+_{g_j}\rho_{g_i g_{j+1}} - c^-_{g_j}\rho_{g_i g_{j-1}} \right\}, \tag{9}$$

where $c^{\pm}_{Fm_F} \equiv \sqrt{(F \mp m_F)(F \pm m_F + 1)}$.

The TMF couples the m_F Zeeman sublevels in increments of $\Delta m_F \pm 1$ and causes redistribution of the population among the Zeeman sublevels, as do the collisional and time-of-flight terms in Eqs. (1) and (3).

From the solution of the Bloch equations, we calculate the absorption of the system. The pump and probe absorption $\alpha(\omega_{1,2})$ is given by [19,20]

$$\alpha(\omega_{1,2}) = \frac{4\pi\omega_0 N}{\hbar c}\sum_{e_i g_j}\frac{|\mu_{e_i g_j}|^2}{V_{e_i g_j}(\omega_{1,2})}\mathrm{Im}[\rho_{e_i g_j}(\omega_{1,2})], \tag{10}$$

where N is the atomic density and ω_0 is the transition frequency in the absence of a magnetic field.

III. THE HANLE CONFIGURATION

A. Analytical solutions of Bloch equations

For the Hanle configuration, we solve the Bloch equations analytically for the $F_g = 1 \rightarrow F_e = 0$ system in the presence of a scanning longitudinal magnetic field B_z and a constant TMF B_x, for a linearly polarized pump whose σ polarization is parallel to the TMF. The pump is resonant with the $|F_g = 1, m_g = 0\rangle \rightarrow |F_e = 0, m_e = 0\rangle$ transition [see Fig. 1(a)]. As the longitudinal magnetic field is scanned, the detunings change such that $\Delta_{eg_1} = -\Delta_{eg_3}$. It can be shown that, in the absence of the TMF, $\rho_{g_1 g_1} = \rho_{g_3 g_3}$, $\rho_{ee} \approx 0$, and $\rho_{eg_1} = -\rho^*_{eg_3}$ [21], and also that $\rho_{g_1 g_2} = -\rho_{g_2 g_3}$ and $\rho_{eg_2} = 0$ [22]. We can show numerically and analytically that these relations still hold even in the presence of the small TMFs considered here, so that the sixteen Bloch equations can be reduced to three equations:

$$\dot{\rho}_{eg_1} = (i\Delta_1 - \Gamma')\rho_{eg_1} + iV\left(\rho_{g_1 g_1} - \rho_{g_3 g_1}\right), \tag{11}$$

$$\dot{\rho}_{g_3 g_1} = (i2\omega - \gamma')\rho_{g_3 g_1} - 2iV\rho_{eg_1} - 2iA\rho_{g_2 g_1}, \tag{12}$$

$$\dot{\rho}_{g_2 g_1} = (i\omega - \gamma')\rho_{g_2 g_1} + iV\rho_{g_2 e} + iA\left(1 - 3\rho_{g_1 g_1} - \rho_{g_3 g_1}\right), \tag{13}$$

where $\omega = \omega_{g_1 g_2} = -\mu_B B_z g_g/\hbar$, $\Delta_1 = \omega_1 - \omega_{eg_1} = \omega_{g_1 g_2} = \omega$, $\Gamma' = \Gamma'_{e_i g_j}$, $\gamma' = \Gamma'_{g_i g_j}$, and $A = \mu_B B_x g_g/\sqrt{2}\hbar$. The steady-state solution of ρ_{eg_1} is given by

$$\rho_{eg_1} = -\frac{iV\rho_{g_1 g_1}}{(i\Delta_1 - \Gamma')}D^{-1} - \frac{2iA^2 V\left(1 - 3\rho_{g_1 g_1}\right)}{(i\Delta_1 - \Gamma')d}D^{-1}, \tag{14}$$

where

$$D = 1 + \frac{2V^2 d + 4A^2 V^2}{(i\Delta_1 - \Gamma')(-2i\omega + \gamma')d}, \tag{15}$$

with

$$d = [(-i\omega + \gamma')(-2i\omega + \gamma') + 2A^2]. \tag{16}$$

When we consider the denominators in Eq. (14), we see from the expression $(i\Delta - \Gamma') = (i\omega - \Gamma')$ that the pump absorption has a maximum when $\omega = 0$ where $B_z = 0$, and we see from the expression for d [see Eq. (16)] that the pump absorption has minima at $\omega = \pm A$ where $B_z = \pm B_x/\sqrt{2}$. We note that the minima occur at the same values of B_z where the population is equally distributed among the Zeeman ground-state sublevels, so that the second term in Eq. (14) becomes zero.

B. Results and discussion of the Hanle effect

In Fig. 2, we show numerical results for the absorption as a function of longitudinal field for a σ polarized resonant laser exciting a realistic closed transition, $F_g = 1 \rightarrow F_e = 0$ of the ^{87}Rb D_2 line (similar results were obtained for the $F_g = 1 \rightarrow F_e = 1$ and $F_g = 2 \rightarrow F_e = 1$ open transitions), in the absence and presence of a TMF. In the absence of the transverse field (solid line), the sublevels of the lower level are all degenerate at $B_z = 0$, leading to two-photon resonance, and CPT is observed. This is reflected in a narrow dip in the broad absorption spectrum at $B_z = 0$.

In the presence of a constant TMF (dashed line), the spectrum of the pump absorption is modified: the narrow CPT dip widens, its amplitude decreases, and it splits into two symmetrically displaced dips at $B_z = \pm B_x/\sqrt{2}$, as predicted analytically. Thus, the distance between the dips increases linearly with B_x (see the inset in Fig. 2). This phenomenon can effectively be implemented in magnetometry, as it allows measurement of the value of the TMF by determining the separation between the dips. Similar results have been shown for the $F_g = 2 \rightarrow F_e = 1$ transition in the ^{87}Rb D_1 line for an elliptically polarized pump [1]. The authors suggest that this effect is due to the creation of high-order ground-state

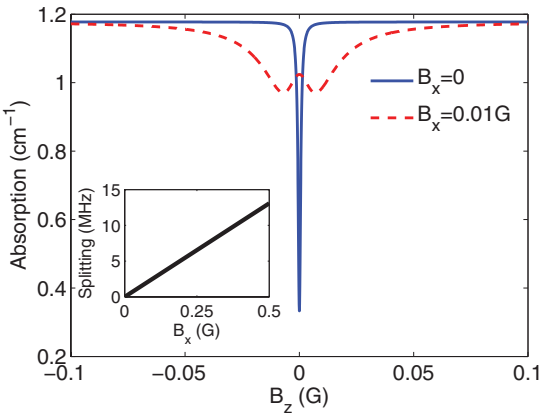

FIG. 2. (Color online) Hanle effect in $F_g = 1 \rightarrow F_e = 0$ of the ^{87}Rb D_2 line. The scanning magnetic field is B_z, and the additional constant transverse magnetic field ($B_x = 0.01$ G) causes the narrow CPT dip to widen and split. The parameters used in the calculation are $\Omega = 6\pi \times 10^6$ s^{-1}, $\Gamma = 2\pi \times 6.0666$ MHz, $\gamma = 10^{-5}\Gamma$, $\Gamma^* = 100\Gamma$, $\Gamma^*_{g_i g_j} = 0$, and $\Gamma_{g_i g_j} = 10^{-5}\Gamma$. When $\Gamma_{g_i g_j} = 0$, the contrast of the splitting is smaller, as the collisional population redistribution reinforces the redistribution caused by the TMF. Inset: The splitting as a function of B_x, calculated numerically with the full Bloch equations.

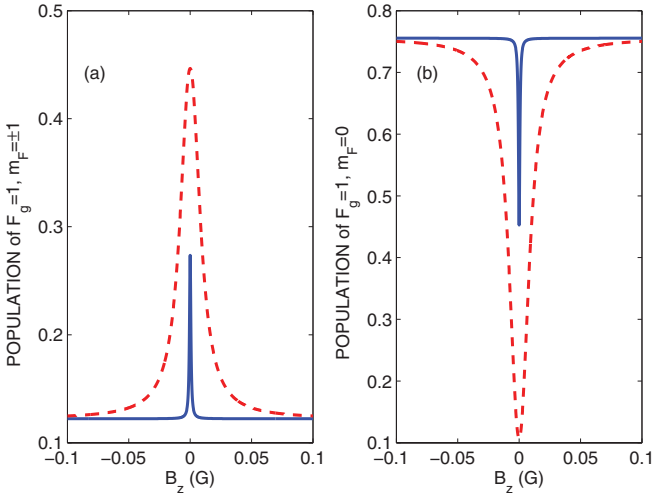

FIG. 3. (Color online) The populations in the (a) $|F_g = 1, m_g = \pm 1\rangle$ and (b) $|F_g = 1, m_g = 0\rangle$ Zeeman sublevels for the same parameters as in Fig. 2, in the absence (solid line) and presence (dashed line) of TMF $B_x = 0.01$ G.

coherences [23], $\Delta m = 4$ in their case, so that it should not be expected to occur for the $F_g = 1 \rightarrow F_e = 0$ transition. However, we show that the splitting does indeed occur for the $F_g = 1 \rightarrow F_e = 0$ transition. This splitting was not seen in the earlier work of [1] due to the absence of collisions in their experimental system. These collisions reinforce the redistribution of the population in the Zeeman sublevels due to the TMF.

Splitting of an EIT dip by a TMF has also been observed for an N system in Rb atoms [24], and splitting of a CPT dip has been observed for a tilted magnetic field in a Rb atomic magnetometer that uses polarization modulation to eliminate "dead zones," that is, orientations of the magnetic field where the magnetometer loses its sensitivity [25].

The redistribution of the population by the combined effects of the TMF and the collisions is illustrated in Fig. 3, in which we see that the population is trapped in the $|F_g = 1, m_g = \pm 1\rangle$ Zeeman sublevels. In Fig. 4, we see that the TMF has created the ground-state coherences $\rho_{g_1 g_2}$ and $\rho_{g_2 g_3}$ that were zero in its absence. In addition, the degree of coherence of the subsystems $S_{g_1 g_2} = S_{g_2 g_3}$, where $S_{g_i g_j} = (\rho_{g_i g_j})^2 / \rho_{g_i g_i} \rho_{g_j g_j}$, is maximum close to the points of the minima in the absorption spectra, whereas $S_{g_1 g_3}$ remains maximum at $B_z = 0$.

In order to explain physically the origin of the splitting, we will consider the problem in the basis set in which the direction of the total magnetic field is the quantization axis of the system [Fig. 1(b)]. We will refer to these ground-state Zeeman sublevels as m'_g to distinguish them from the m_g basis discussed above, where the quantization is in the z direction [Fig. 1(a)]. In the absence of a TMF, the quantization axis is aligned along the z axis. The light propagates in the z direction, so that the laser polarization can be considered as purely σ. However, in the presence of a constant TMF, the direction of the quantization axis changes as B_z is scanned, so that the laser polarization also changes. Thus, the polarization is no longer purely σ but is a combination of σ and π.

At $B_z = 0$, in the presence of a TMF, the laser is purely π polarized, leading to absorption in the $|F_g = 1, m_g = 0\rangle \rightarrow |F_e = 0, m_e = 0\rangle$ transition. This is reflected in the absorption peak that appears when $B_z = 0$ (the dashed line in Fig. 2).

When $B_z \neq 0$, σ polarization is added to the π polarization, leading to two additional two-photon detuned Λ subsystems: $|F_g = 1, m'_g = -1\rangle \leftrightarrow |F_e = 0, m'_e = 0\rangle \leftrightarrow |F_g = 0, m'_g = 0\rangle$ and $|F_g = 1, m'_g = 1\rangle \leftrightarrow |F_e = 0, m'_e = 0\rangle \leftrightarrow |F_g = 0, m'_g = 0\rangle$. As B_z increases, the transitions that interact with the σ polarization become more detuned due to the increase in the Zeeman splitting of the m'_g sublevels. On the other hand, the relative intensity of the σ polarized component of the light increases. When the σ polarized component of

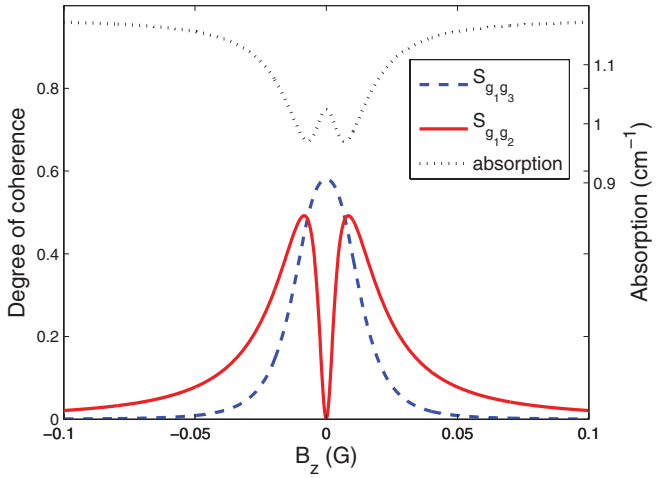

FIG. 4. (Color online) Degree of coherence calculated numerically from the full Bloch equations for the same parameters as in Fig. 2, in the presence of a TMF ($B_x = 0.01$G). $S_{g_1 g_2}$ is maximum close to the points of the minima in the absorption spectra, whereas $S_{g_1 g_3}$ has a higher maximum at $B_z = 0$.

the light is sufficiently strong, the two competing effects lead to a region where two-photon detuned CPT occurs. We verified this description by considering a simple Λ system in which the field interacting with one of the legs gradually becomes stronger and more detuned while the other field remains at resonance but gradually becomes weaker. As B_x increases, the absorption spectrum becomes broader and weaker until the splitting becomes indiscernible. In this picture [Fig. 1(b)], the system is similar to the tripod system in which the $F_g = 1 \rightarrow F_e = 0$ transition interacts with a σ polarized pump and a π polarized probe [22,26]. The same phenomenon occurs for the $F_g = 2 \rightarrow F_e = 1$ transition where the TMF leads to the formation of a multitripod system [27,28].

IV. PUMP-PROBE CONFIGURATION

A. Analytical solutions of Bloch equations

As in the case of the Hanle configuration, we analytically solve the Bloch equations for the pump-probe configuration for the $F_g = 1 \rightarrow F_e = 0$ system for a σ^+ polarized pump resonant with the $|F_g = 1, m_g = 0\rangle \rightarrow |F_e = 0, m_e = 0\rangle$ transition and a scanning σ^- polarized probe in the presence of constant longitudinal and transverse magnetic fields.

Based on the assumptions given in Sec. III A, the 16 Bloch equations can be reduced to the following three equations:

$$\dot{\rho}_{eg_3} = [i(\Delta_2 - \delta) - \Gamma']\rho_{eg_3} + iV\left(\rho_{g_1g_3} + \rho_{g_3g_3}\right), \quad (17)$$

$$\dot{\rho}_{g_1g_3} = [i(\Delta_2 - 2\delta) - \gamma']\rho_{g_1g_3} + 2iV\rho_{eg_3} - iA\left(\rho_{g_2g_3} - \rho_{g_1g_2}\right), \quad (18)$$

$$\dot{\rho}_{g_1g_2} = [i(\Delta_2/2 - \delta) - \gamma']\rho_{g_1g_2} + iV\rho_{eg_2} - iA\left(1 - 3\rho_{g_3g_3} - \rho_{g_1g_3}\right), \quad (19)$$

where $\Delta_2 = \omega_2 - \omega_{eg_2}$ and $\delta = \mu_B B_z g_g/\hbar$. Note that in the Hanle configuration ω_1 is fixed and Δ_1 changes with B_z, whereas in the pump-probe configuration ω_1 and B_z are fixed and Δ_2 varies with ω_2. The steady-state solution of ρ_{eg_3} is given by

$$\rho_{eg_3} = -\frac{iV\rho_{g_3g_3}}{i(\Delta_2 - \delta) - \Gamma'}D^{-1} - \frac{2iA^2V\left(1 - 3\rho_{g_3g_3}\right)}{[i(\Delta_2 - \delta) - \Gamma']d}D^{-1}, \quad (20)$$

where

$$D = \frac{\{[i(\Delta_2 - \delta) - \Gamma'][i(\Delta_2 - 2\delta) - \gamma'] + 2V^2\}d - 4A^2V^2}{[i(\Delta_2 - \delta) - \Gamma'][i(\Delta_2 - 2\delta) - \gamma']d}, \quad (21)$$

with

$$d = \{[(i\Delta_2/2 - \delta) - \gamma'][i(\Delta_2 - 2\delta) - \gamma'] + 2A^2\}. \quad (22)$$

When we consider the denominators in Eq. (20), we see from the expression $i(\Delta_2 - \delta) - \Gamma'$ that the pump absorption has a maximum when $\Delta_2 = 0$, and we see from the expression for d [see Eq. (22)] that the pump absorption has minima at $\Delta_2 = 2\delta \pm 2A$. It is interesting to note that B_x and B_z have independent effects on the positions of the minima.

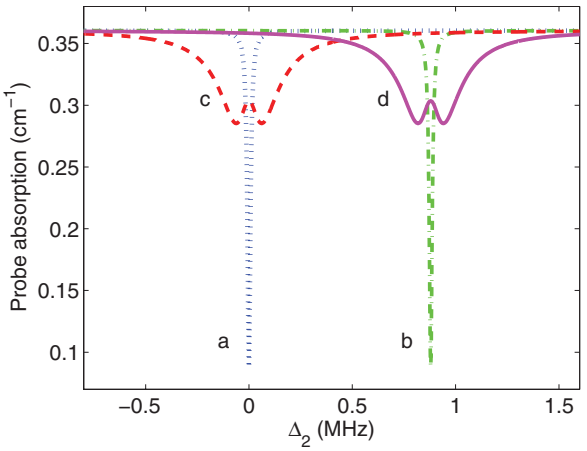

FIG. 5. (Color online) Probe absorption in the realistic system $F_g = 1 \rightarrow F_e = 0$ of the ^{87}Rb D_2 line for different values of the longitudinal and transverse magnetic fields. (a) Dotted line: $B_z = 0$ and $B_x = 0$. (b) Dot-dashed line: $B_z = 0.1$ G and $B_x = 0$. (c) Dashed line: $B_z = 0$ and $B_x = 0.01$ G. (d) Continuous line: $B_z = 0.1$ G and $B_x = 0.01$ G. The parameters used in the calculation are $\Omega = 6\pi \times 10^6$ s^{-1}, $\Gamma = 2\pi \times 6.067$ MHz, $\gamma = 10^{-5}\Gamma$, $\Gamma^* = 100\Gamma$, $\Gamma^*_{g_ig_j} = 0$, and $\Gamma_{g_ig_j} = 10^{-5}\Gamma$.

B. Results and discussion of the pump-probe configuration

In Fig. 5, we show numerical results for the probe absorption in the realistic system $F_g = 1 \rightarrow F_e = 0$ of the ^{87}Rb D_2 line for a σ^+ polarized pump and a scanning σ^- polarized probe for different values of the longitudinal and transverse magnetic fields (similar results are obtained for the $F_g = 1 \rightarrow F_e = 1$ and $F_g = 2 \rightarrow F_e = 1$ systems). In the absence of any magnetic field (case a), the CPT dip is centered at $\Delta = 0$. When only a longitudinal magnetic field is applied (case b), Zeeman splitting of the ground hyperfine state occurs and the CPT dip is shifted to $\Delta_2 = 2\delta = 2\mu_B g_g B_z$. When only a transverse magnetic field exists (case c), the CPT dip widens and is split into two with reduced amplitude. When both of the fields are present (case d), the CPT dip is both shifted and split. Generally, we can say that B_z determines the general shift of the CPT dip, while B_x causes the splitting of the dip. As predicted analytically, the longitudinal and the transverse magnetic fields lead to two different independently measurable phenomena. Thus, this effect can be applied successfully in vector magnetometry.

If we set the quantization axis to be along the total magnetic field, in the pump-probe configuration the direction of the quantization axis is constant and determined by the fixed longitudinal and transverse magnetic fields, unlike the Hanle configuration, in which the direction of the quantization axis varies as a function of the scanned field. The longitudinal magnetic field shifts the Zeeman sublevels in energy but does not change the laser polarization, which remains purely σ^+ for the pump and σ^- for the probe. The TMF, however, in addition to the shift in energy of the Zeeman sublevels, changes the laser polarization from pure σ^+ and σ^- to a combination of σ^+, σ^-, and π polarizations, thereby creating two new Λ subsystems which lead to the two dips in the absorption spectrum.

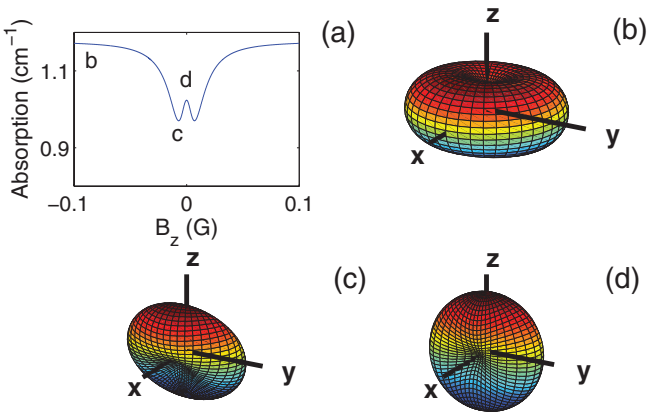

FIG. 6. (Color online) The AMPS at various values of B_z in the Hanle type spectrum of Fig. 2. (a) Pump absorption in the Hanle configuration in the presence of $B_x = 0.01$G (the same spectrum as in Fig. 2), (b) far from resonance ($|B_z| > 0$), (c) near the minima at $B_z = \pm B_x/\sqrt{2}$, (d) at resonance ($B_z = 0$).

V. ANGULAR MOMENTUM PROBABILITY SURFACE (AMPS)

The ground-state coherence created in the presence of the TMF can be illustrated using the angular momentum probability surface (AMPS) [29], whose radius in a given direction is determined by the probability of measuring the maximum possible angular momentum projection in that direction.

The AMPS evolution of a CPT process in the pump-probe configuration for a fixed pump as a function of the probe detuning in the absence of a magnetic field (which is equivalent to scanning B_z in the Hanle configuration) has been illustrated in a movie by Rochester and Budker [30]. There, we see that when the probe is far from resonance there is almost no coherence between the Zeeman sublevels and due to optical pumping most of the population is concentrated in the $|F_g = 1, m_g = 0\rangle$ sublevel, causing the AMPS to resemble a "doughnut" aligned along the z axis. As the probe approaches resonance, the ground-state coherence $\rho_{g_1g_3}$ increases so that the probability distribution now resembles a "peanut" along the x axis.

In Fig. 6, we show the AMPS for various values of B_z in the Hanle type spectrum of Fig. 2 [31]. Here, the AMPS evolution of the CPT process is affected by the ground-state coherences between neighboring sublevels that are created by the TMF. Far from resonance ($|B_z| > 0$), there is no significant change from the case of the CPT process in the absence of TMF, so that the AMPS has the same doughnut shape aligned along the z axis. Near the minima at $B_z = \pm B_x/\sqrt{2}$, the AMPS has a doughnut shape tilted with respect to the z axis. At this point, the population is equally distributed among the Zeeman sublevels, and the amplitudes of the coherences between the various sublevels are approximately equal ($\rho_{g_1g_2} \approx -\rho_{g_2g_3} \approx \rho_{g_1g_3} \approx -1/3$). If all the coherences were zero, the AMPS would be spherical (the unpolarized state), and, if only the coherence between the extreme levels were nonzero, the AMPS would be peanut shaped along the x axis, as in the case of CPT. On the other hand, if only the coherences between neighboring states existed, the peanut would be tilted with respect to the z axis. When all the coherences are present, the peanut turns into a doughnut with the same tilt. At resonance ($B_z = 0$), the population is in the extreme levels and the only nonzero coherence is between these levels. This results in a doughnut-shaped AMPS aligned along the x axis.

VI. CONCLUSIONS

The effect of a TMF on the absorption spectra of degenerate two-level systems (DTLSs) of the ^{87}Rb D_2 line has been analyzed both analytically and numerically. We compared the effect of the TMF on the absorption of a σ polarized pump in the Hanle configuration with that of a σ^- probe in the presence of a σ^+ pump in the pump-probe configuration, and we showed that the absorption spectra in both the Hanle and pump-probe configurations are split in the presence of a TMF and that the splitting is proportional to the magnitude of the TMF. We note that the splitting is more marked in the presence of collisions that reinforce the effect of population redistribution due to the TMF.

In our calculations, we set the axis of light propagation to be the quantization axis. This gives the same results as setting the quantization axis in any other arbitrary direction. The change in the effective light polarization in the case in which the quantization axis is set along the total magnetic field leads to the creation of new two-photon detuned Λ subsystems formed by the Zeeman sublevels. There are two competing effects that lead to a region where two-photon detuned CPT occurs. In addition to being split, the CPT dip in the pump-probe configuration is shifted by the longitudinal magnetic field. Thus, we find that the effects of longitudinal and transverse magnetic fields can be distinguished from each other; that is, the value and sign of B_z and the value of B_x can be determined separately. In the future, we will investigate the effect of adding B_y to the already existing magnetic fields, in order to explore the possibility of achieving vector magnetometry with all components of the magnetic field.

ACKNOWLEDGMENTS

We are grateful to D. Budker and F. Renzoni for stimulating discussions.

[1] A. Huss, R. Lammegger, L. Windholz, E. Alipieva, S. Gateva, L. Petrov, E. Taskova, and G. Todorov, Opt. Soc. Am. B **23**, 1729 (2006).

[2] K. Nasyrov, S. Cartaleva, N. Petrov, V. Biancalana, Y. Dancheva, E. Mariotti, and L. Moi, Phys. Rev. A **74**, 013811 (2006).

[3] V. Polischuk, L. Petrov, D. Slavov, V. Domelunksen, and G. Todorov, SPIE **6257**, 62570A (2006).

[4] Y. J. Yu, H. J. Lee, I. H. Bae, H. R. Noh, and H. S. Moon, Phys. Rev. A **81**, 023416 (2010).

[5] H. R. Noh and H. S. Moon, Phys. Rev. A **82**, 033407 (2010).

[6] N. Ram, M. Pattabiraman, and C. Vijayan, Phys. Rev. A **82**, 033417 (2010).
[7] F. Renzoni, S. Cartaleva, G. Alzetta, and E. Arimondo, Phys. Rev. A **63**, 065401 (2001).
[8] J. Dimitrijevic, A. Krmpot, M. Mijailovic, D. Arsenovic, B. Panic, Z. Grujic, and B. M. Jelenkovic, Phys. Rev. A **77**, 013814 (2008).
[9] N. Ram and M. Pattabiraman, J. Phys. B **43**, 245503 (2010).
[10] H.-J. Kim and H. S. Moon, Opt. Exp. **19**, 168 (2011).
[11] D. Brazhnikov, A. Taichenachev, A. Tumaikin, V. Yudin, I. Ryabtsev, and V. Entin, JETP Lett. **91**, 625 (2010).
[12] V. I. Yudin, A. V. Taichenachev, Y. O. Dudin, V. L. Velichansky, A. S. Zibrov, and S. A. Zibrov, Phys. Rev. A **82**, 033807 (2010).
[13] C. Goren, A. D. Wilson-Gordon, M. Rosenbluh, and H. Friedmann, Phys. Rev. A **67**, 033807 (2003).
[14] T. Zigdon, A. D. Wilson-Gordon, S. Guttikonda, E. J. Bahr, O. Neitzke, S. M. Rochester, and D. Budker, Opt. Exp. **18**, 25494 (2010).
[15] K. Cox, V. I. Yudin, A. V. Taichenachev, I. Novikova, and E. E. Mikhailov, Phys. Rev. A **83**, 015801 (2011).
[16] F. Renzoni, W. Maichen, L. Windholz, and E. Arimondo, Phys. Rev. A **55**, 3710 (1997).
[17] A. D. Wilson-Gordon and H. Friedmann, Opt. Lett. **14**, 390 (1989).
[18] A. D. Wilson-Gordon, Phys. Rev. A **48**, 4639 (1993).
[19] S. Menon and G. S. Agarwal, Phys. Rev. A **59**, 740 (1999).
[20] R. W. Boyd, *Nonlinear Optics*, 2nd ed. (Academic, San Diego, 2003).
[21] S. Boublil, A. D. Wilson-Gordon, and H. Friedmann, J. Mod. Opt. **38**, 1739 (1991).
[22] C. Goren, A. D. Wilson-Gordon, M. Rosenbluh, and H. Friedmann, Phys. Rev. A **69**, 063802 (2004).
[23] A. B. Matsko, I. Novikova, M. S. Zubairy, and G. R. Welch, Phys. Rev. A **67**, 043805 (2003).
[24] V. Entin, I. Ryabtsev, A. Boguslavskii, and I. Beterov, JETP Lett. **71**, 175 (2000).
[25] A. Ben-Kish and M. V. Romalis, Phys. Rev. Lett. **105**, 193601 (2010).
[26] N. Gavra, M. Rosenbluh, T. Zigdon, A. D. Wilson-Gordon, and H. Friedmann, Opt. Comm. **280**, 374 (2007).
[27] R. Meshulam, T. Zigdon, A. D. Wilson-Gordon, and H. Friedmann, Opt. Lett. **32**, 2318 (2007).
[28] A. M. Akulshin, S. Barreiro, and A. Lezama, Phys. Rev. A **57**, 2996 (1998).
[29] M. Auzinsh, D. Budker, and S. M. Rochester, *Optically Polarized Atoms: Understanding Light-Atom Interactions*, 1st ed. (Oxford University Press, Oxford, 2010).
[30] S. M. Rochester and D. Budker at http://budker.berkeley.edu/ADM/eitamps_24fps.mov.
[31] See Supplemental Material at http://link.aps.org/supplemental/10.1103/PhysRevA.87.033808 for a movie of the complete spectrum.